chemosensors

MDPI

Article

Study on Hybrid Assemblies of Graphene and Conducting Polymers with Embedded Gold Nanoparticles for Potential Electrode Purposes

Alexandru F. Trandabat [1], Oliver Daniel Schreiner [1,2], Thomas Gabriel Schreiner [2], Olga Plopa [1] and Romeo Cristian Ciobanu [1,*]

[1] Department of Electrical Measurements and Materials, Gheorghe Asachi Technical University, 700050 Iasi, Romania; ftranda@tuiasi.ro (A.F.T.); oliver090598@yahoo.com (O.D.S.); lesea_ro@yahoo.com (O.P.)
[2] Department of Medical Specialties III, Faculty of Medicine, University of Medicine and Pharmacy "Grigore T. Popa", 700115 Iasi, Romania; schreiner.thomasgabriel@yahoo.com
* Correspondence: r.c.ciobanu@tuiasi.ro

Abstract: This article outlines the method of creating electrodes for electrochemical sensors using hybrid nanostructures composed of graphene and conducting polymers with insertion of gold nanoparticles. The technology employed for graphene dispersion and support stabilization was based on the chemical vapor deposition technique followed by electrochemical delamination. The method used to obtain hybrid nanostructures from graphene and conductive polymers was drop-casting, utilizing solutions of P3HT, PANI-EB, and F8T2. Additionally, the insertion of gold nanoparticles utilized an innovative dip-coating technique, with the graphene-conducting polymer frameworks submerged in a $HAuCl_4$/2-propanol solution and subsequently subjected to controlled heating. The integration of gold nanoparticles differs notably, with P3HT showing the least adhesion of gold nanoparticles, while PANI-EB exhibits the highest. An inkjet printer was employed to create electrodes with metallization accomplished through the use of commercial silver ink. Notable variations in roughness (grain size) result in unique behaviors of these structures, and therefore, any potential differences in the sensitivity of the generated sensing structures can be more thoroughly understood through this spatial arrangement. The electrochemical experiments utilized a diluted sulfuric acid solution at three different scan rates. The oxidation and reduction potentials of the structures seem fairly alike. Nevertheless, a notable difference is seen in the anodic and cathodic current densities, which appear to be largely influenced by the active surface of gold nanoparticles linked to the polymeric grains. The graphene–PANI-EB structure with Au nanoparticles showed the highest responsiveness and will be further evaluated for biomedical applications.

Keywords: graphene; conducting polymers; gold nanoparticles; electrochemical sensors

check for updates

Received: 20 January 2025
Revised: 21 March 2025
Accepted: 2 April 2025
Published: 4 April 2025

Citation: Trandabat, A.F.; Schreiner, O.D.; Schreiner, T.G.; Plopa, O.; Ciobanu, R.C. Study on Hybrid Assemblies of Graphene and Conducting Polymers with Embedded Gold Nanoparticles for Potential Electrode Purposes. *Chemosensors* **2025**, *13*, 130. https://doi.org/10.3390/chemosensors13040130

Copyright: © 2025 by the authors. Licensee MDPI, Basel, Switzerland. This article is an open access article distributed under the terms and conditions of the Creative Commons Attribution (CC BY) license (https://creativecommons.org/licenses/by/4.0/).

1. Introduction

The electrochemical sensor is a common type of sensing device that converts biochemical events into electrical signals. In this kind of sensor, the working electrode is an essential element used as a solid base for the immobilization of biomolecules and the transfer of electrons. Owing to various nanomaterials with significant surface area, synergistic effects are facilitated by enhancing loading capacity and the mass transport of reactants, leading to improved performance in analytical sensitivity. The carbon allotropes can serve as electrodes and supporting scaffolds because of their extensive active surface

area and efficient electron transfer rate. Conducting polymers represent other significant category of functional materials that have been extensively utilized in the production of electrochemical sensors, due to their adjustable chemical, electrical, and structural characteristics. Conducting polymers can also be engineered with other functional materials like nanoparticles to significantly enhance the sensitivity and selectivity of the sensor's reaction to various analytes. In recent years, hybrid materials made of graphene and different polymers have been thoroughly studied, considered to lead to considerable progress in electrochemical sensing. The creation of such hybrid nanostructures is associated with their unique electrical properties.

A method for producing graphene/polyaniline, graphene/poly(3,4-ethylene dioxythiophene), and graphene/polypyrrole (PPy) nanocomposites is highlighted in [1]. A detailed overview of various hybrid structures comprising metallic oxides, graphene, and conductive polymers like poly-indole, polypyrrole, and poly-aniline is provided in [2]. A review of analogous structures of graphene oxide/conducting polymer composites, now presented as hydrogels, is provided in [3]. Similar technologies are noted in additional sources [4–9]. The main use of hybrid structures made from graphene and conducting polymers is related to sensors. In the last 15 years, numerous sensors have been developed, starting from simple types like those for humidity [10,11], temperature [12], and gas detection [13–17], which also include waste gas evaluation [18] and various chemical sensors [19,20]; advancing to sensors with multiple applications for detecting dopamine, serotonin, cholesterol, bilirubin, uric acid, and others [21–26]; as well as specialized sensors for environmental monitoring that identify pollutants in water, such as heavy metals [27,28]; and finishing with examinations of food and pharmaceutical products [29,30].

A new research direction in the field of sensors involves integrating metallic nanostructures into the architecture of conducting polymers to improve the sensitivity and/or selectivity of sensors, as detailed in [31–35], with applications tested for impedimetric, electrochemical, or chemosensors. However, no research has so far attempted to improve the characteristics of sensors by incorporating gold nanoparticles into more complex structures, even if the advantage of simple use of gold nanoparticles for sensor application was noticed by some authors in recent studies [36,37]. Therefore it is worthwhile to further investigate the development of electrodes featuring more intricate structures that incorporate gold nanoparticles. Various techniques for integrating gold nanoparticles into polymer frameworks are extensively discussed in the literature, such as: drop-casting, dip-coating or in-situ synthesis and integration, [38–40], but the paper introduced an innovative approach in this domain based on dip-coating method.

The significance of this study lies in creating functional electrodes for electrochemical sensing systems by embedding gold nanoparticles within hybrid assemblies of graphene and conducting polymers, a complexity of materials for electrodes not previously detailed in the literature. An effective technique for incorporating gold nanoparticles into the surface of conducting polymers was presented, involving the immersion of the polymer film in a highly diluted $HAuCl_4$ solution, followed by controlled heating, resulting in a substantial impact on a broader surface, potentially serving as a working electrode. Three hybrid structures were analyzed, ultimately determining which one was the optimal selection based on responsive features evaluated through cyclic voltammetry.

2. Materials, Preparation and Characterizing Methods

2.1. Materials and Preparation Methods for Graphene Substate

The technology used for graphene synthesis, dispersion and support stabilization was widely describe in [41], and was based on the chemical vapor deposition method followed

by an electrochemical delamination. The optimal process, by examining the outcomes achieved at 900 °C and correspondingly 950 °C as detailed in [41], was achieved at 950 °C, leading to enhanced grain structure and the formation of layers mainly characterized by peaks rather than hollows. The samples were ultimately moved onto a SiO_2/Si substrate, because a nonmetallic support allows a more efficient treatment with conducting polymers and can finally generate a functional precursor for an electrochemical electrode. The graphene structures resulted uniform and free from structural defects. The grain size ranged from 1.5 μm and the peak density was reduced, resulting in an improved equilibrium between peaks and hollows.

2.2. Materials and Preparation Methods for Hybrid Nanostructures from Graphene and Conducting Polymers

The method used for creating hybrid nanostructures from graphene and conducting polymers was drop-casting, and five samples of each type were created to evaluate technological feasibility, as widely described in [41]. For Poly 3-hexylthiophene (P3HT), 15 mg/mL of the polymer was dissolved in $CHCl_3$ at room temperature using an ultrasonic bath and allowed to sit for 30 min to achieve a uniform dispersion. In the case of Polyaniline emeraldine-base (PANI-EB), a 20 mg/mL polymer solution was prepared in N-methyl pyrrolidinone (NMP) by dissolving it at room temperature with an ultrasonic bath and allowing it to rest for 30 min for uniform distribution. For Poly[(9,9-dioctylfluorenyl-2,7-diyl)-co-bithiophene] (F8T2), a 20 mg/mL polymer solution was prepared in toluene at 60 °C using an ultrasonic bath and allowed to disperse uniformly for 30 min.

In all instances, 120 μL of each polymer solution was applied to graphene (SiO_2/Si substrate) via the drop-casting technique with Pasteur pipettes. The evaporation of each solvent occurred for 30 min under vacuum conditions, utilizing a Pfeiffer vacuum pump linked to a desiccator.

2.3. Materials and Preparation Methods for Embedding Au Nano-Particles Within Hybrid Graphene-Polymer Structures

The graphene-conductive polymer composite structures were impregnated with a $HAuCl_4$/2-propanol solution by the dip-coating method. The samples were completely immersed and kept for 24 h in a diluted $HAuCl_4$/2-propanol solution (0.001 M). After impregnation, the samples were dried in an oven at 150 °C in a stream of Ar (100 sccm) for 30 min. The system was then cooled to room temperature in a stream of Ar. As shown below, Au nanoparticles with an average size of 100 nm were quasi-uniformly integrated into the hybrid graphene-polymer structures. This approach for obtaining pre-defined Au nanoparticles from a very diluted $HAuCl_4$ solution on the polymeric substrate, heated from room temperature to slightly above one hundred degrees Celsius, is similar to those detailed in [42,43], in those instances handling with remnants of a droplet of $HAuCl_4$ solution and following the same process of heating. But this technique, introduced by the paper, using immersion of the polymer film in a very diluted $HAuCl_4$ solution, has the advantage of creating and quasi-uniformly dispersing gold nanoparticles on larger surfaces, along with several extra advantages: (1) the cost of generating gold nanoparticles is low; (2) the method is simple; (3) no waste liquid is produced following the synthesis of gold nanoparticles.

2.4. Characterization Equipment

Scanning electron microscopy (SEM) and energy-dispersive X-ray spectroscopy (EDX) were performed with a field emission and focused ion beam scanning electron microscope Lyra III XMU (TESCAN GROUP a.s., Brno-Kohoutovice, Czech Republic).

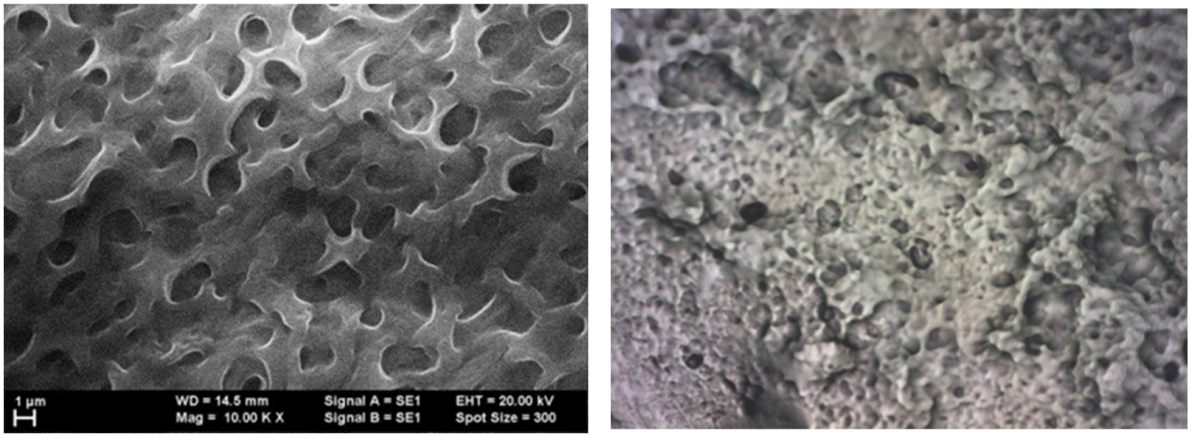
Optical analysis using atomic force microscopy (AFM) was conducted with a Dimension Edge device (Bruker, Billerica, USA). The assessment of roughness was performed using these derived parameters: Ra = Average Roughness; RSk = Skewness; RMS = Root Mean Square Roughness; RKu = Kurtosis. The outcomes for the roughness parameters are shown as averages for 4 scanned regions on each type of sample. The surface roughness parameters are described according to ISO 21920-2:2021 [44,45].

A PARSTAT 4000 potentiostat/galvanostat device (AMETEK Scientific Instruments Inc., Oak Ridge, TN, USA) along with its associated software linked to a computer via the VersaStudio electrochemistry graphical interface was used to assess electrochemical features of samples. Its K0264 Micro-Cell Kit was used as electrochemical cell assembly.

3. Results and Discussion

3.1. AFM Analysis

Along with the initial analysis presented in [41], a SEM analysis was also introduced for all hybrid structures of graphene-conducting polymers. In the case of graphene covered with P3HT, although, at first glance, it seems to have a fairly uniform grain distribution, Figure 1a), when relaying to the image at 500× Figure 1b), it can be noticed that the roughness is quite high. Grains of different sizes but also smoother stretches can be observed, Figure 2.



(**a**) (**b**)

Figure 1. Optical analysis of graphene–P3HT: (**a**) SEM at 10 kx and (**b**) optical at 500×.

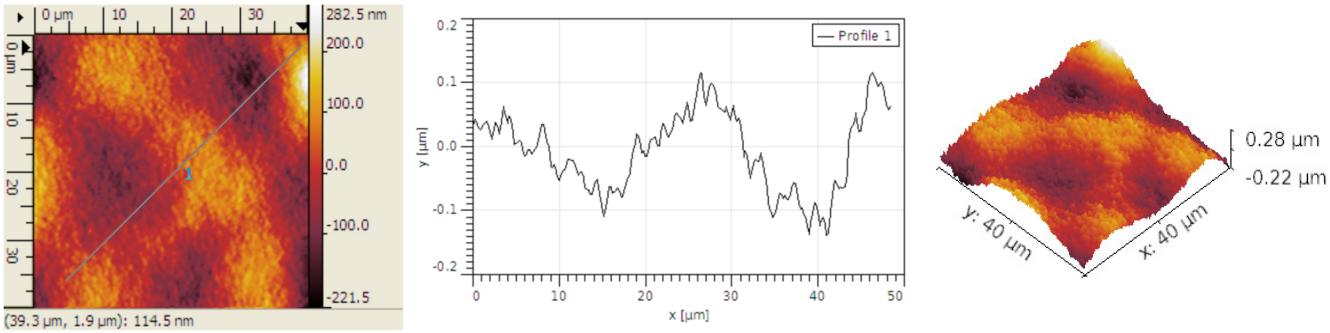


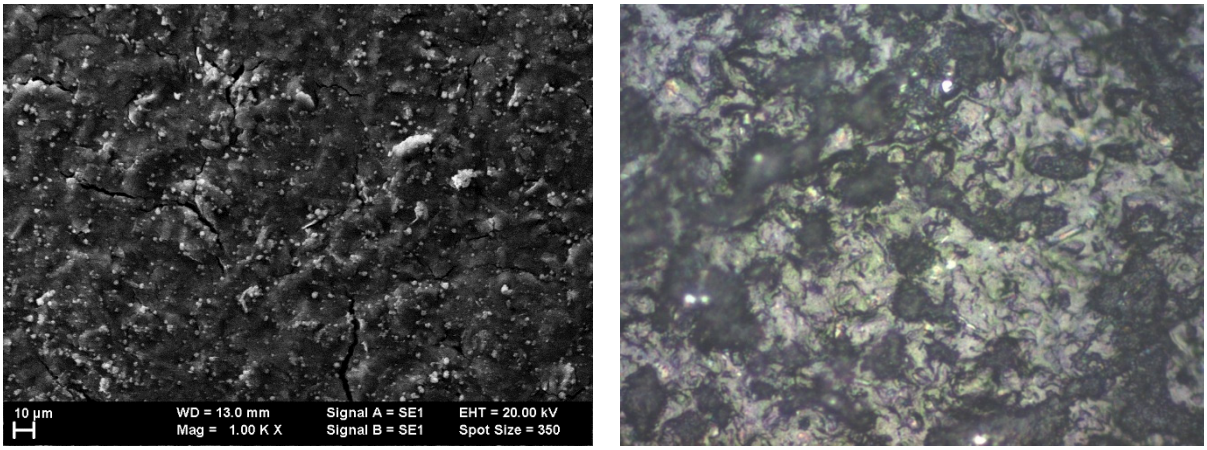
Figure 2. AFM Topographic image and profile lines for graphene–P3HT.

The grain size is small, typically below 0.3 µm. The grains are typically organized in bigger groups. The Rku values are near 3, Table 1, indicating that the grain distribution is fairly symmetrical. The Rsk values are minimal, and we can approximate a roughly equal percentage of peaks and hollow distributed across the surface.

Table 1. Average roughness parameters determined by AFM lines: graphene—P3HT.

Scanned Area	RMS (nm)	Ra (nm)	R_{Sk}	R_{Ku}
40 × 40 µm	64	53	0.143	3.31

In the case of graphene covered with PANI-EB, we can evaluate a roughly equal percentage of peaks and valleys distributed across the surface, but here the grains are organized in smaller groups and present a higher density, Figure 3. The grain size is larger, typically over 2.2 µm, Figure 4, and their concentration is heightened. The Rku values remained near 3, indicating that the grain distribution is symmetrical. The Rsk values are also minimal, comparable with the values for graphene–P3HT structures, suggesting that polymer deposition creates a similar architecture, see Table 2.



(**a**) (**b**)

Figure 3. Optical analysis of graphene–PANI-EB: (**a**) SEM at 1 kx and (**b**) optical at 500×.

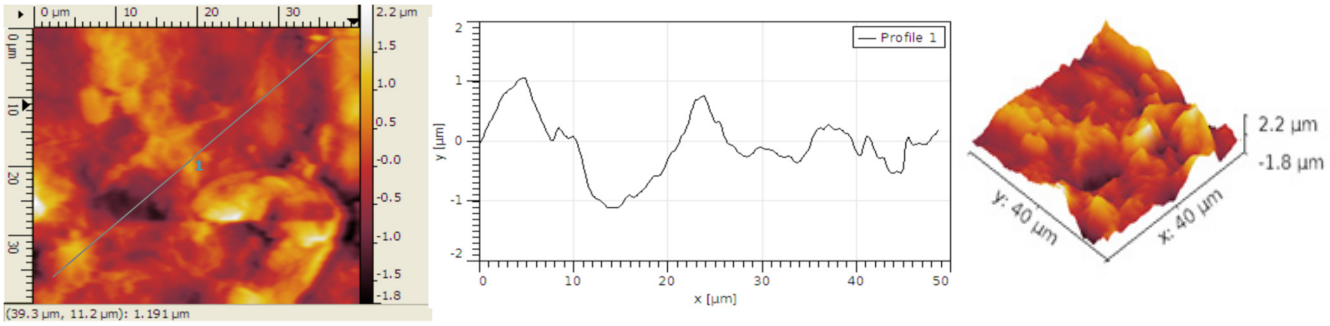
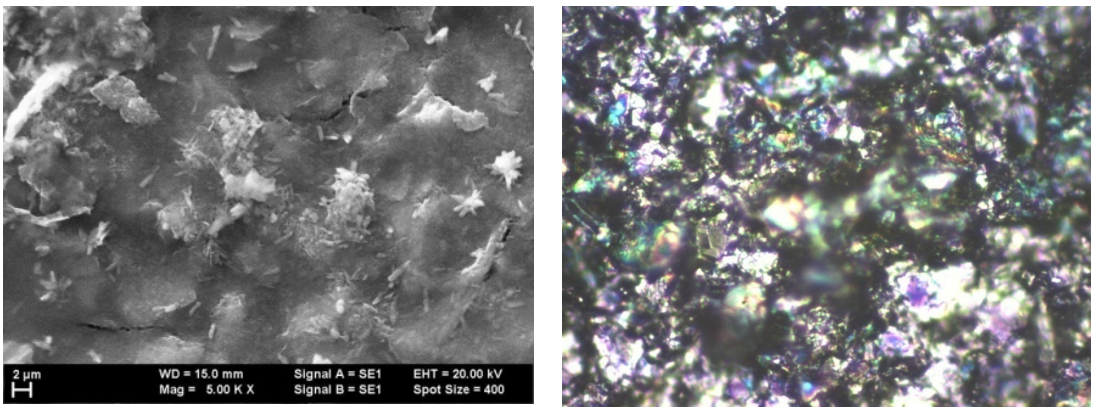


Figure 4. AFM Topographic image and profile lines for graphene–PANI-EB.

Table 2. Average roughness parameters determined by AFM lines: graphene—PANI-EB.

Scanned Area	RMS (nm)	Ra (nm)	R_{Sk}	R_{Ku}
40 × 40 µm	522	414	0.16	3.16

In the case of graphene covered with F8T2, a different topography is observed compared to the structures presented above. Analyzing Figure 5, even if it seems to present a fairly uniform grain distribution, the roughness is much higher compared to the graphene deposited with P3HT or PANI-EB. The grains are arranged less uniformly, and there are grains of different sizes separated by smoother stretches.



(**a**) (**b**)

Figure 5. Optical analysis of graphene–F8T2: (**a**) SEM at 5 kx and (**b**) optical at 500×.

The grain size is generally 3 µm, Figure 6, about 10 times larger compared to the graphene deposited with P3HT, where the grain dimension was 0.28 µm. But the grain size for graphene–F8T2 assembly is in line with the dimension for graphene deposited with PANI-EB, of 2.2 µm. The grains are generally arranged in smaller clusters, and according to the values of R_{Sk} and R_{ku} the grain distribution is quite symmetrical, Table 3.

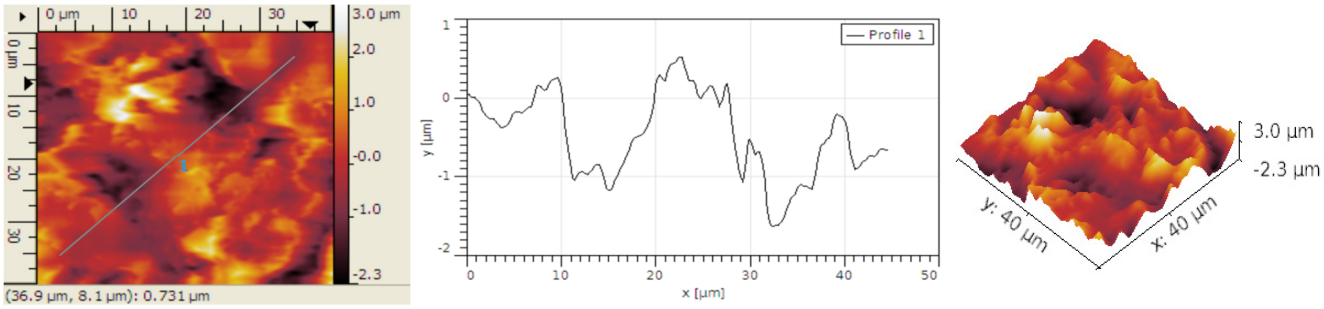


Figure 6. AFM Topographic image and profile lines for graphene–F8T2.

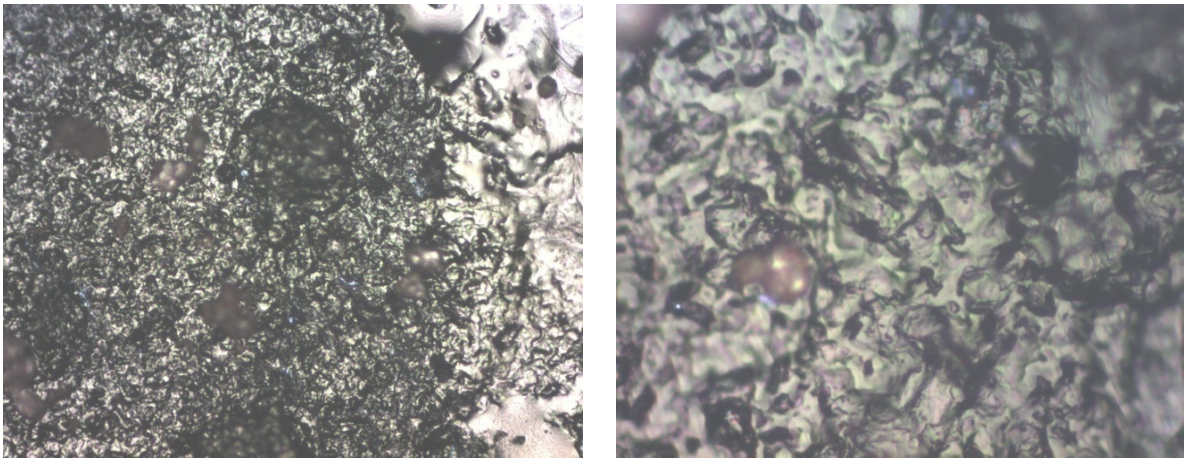
Table 3. Average roughness parameters determined by AFM lines—graphene–F8T2.

Scanned Area	RMS (nm)	Ra (nm)	R_{Sk}	R_{Ku}
40 × 40 µm	705	546	0.191	3.36

In all, AFM emphasized a higher roughness in the case of F8T2 compared to P3HT or PANI-EB, and a larger dimension of grain size.

The analysis of the structure obtained after inserting Au nanoparticles within graphene–P3HT assembly is presented in Figure 7. The existence of gold as quasi-spherical particles with the average dimension of approx. 100 nm is easily observable. However, at first glance, the number of gold particles bonded to the polymer is quite minimal.

The grain size typically measures 0.48 µm, consistent with the size of graphene deposited with PANI-EB without the addition of Au, as shown in Figure 8. The grains are usually organized in smaller groups too. The R_{Sk} values are elevated, suggesting the formation of distinct hollows post-Au deposition; however, the structure of these hollows is scattered due to the limited number of Au particles. The R_{ku} values exceed 4, indicating that the grain symmetry is somewhat altered by the addition of Au, as shown in Table 4.



(**a**) (**b**)

Figure 7. Optical analysis of graphene–P3HT+Au: (**a**) at 100× and (**b**) at 500×.

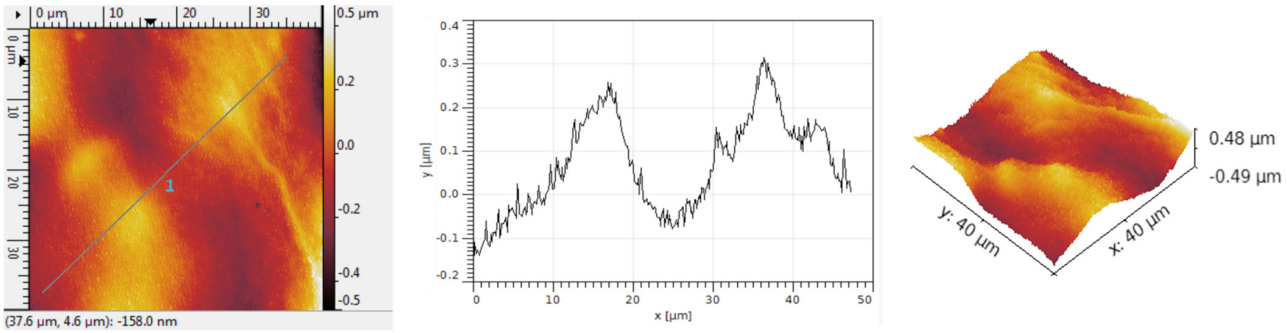
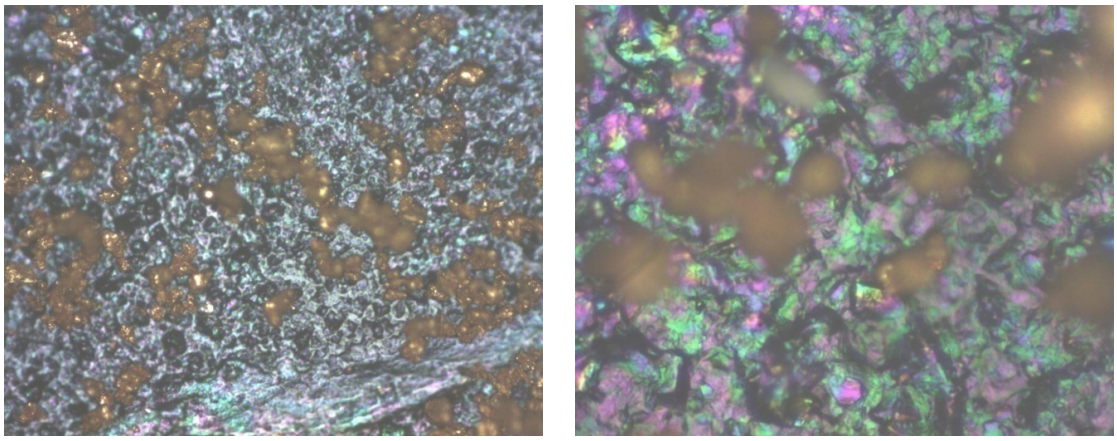


Figure 8. AFM Topographic image and profile lines for graphene–P3HT+Au.

Table 4. Average roughness parameters determined by AFM lines: graphene—P3HT+Au.

Scanned Area	RMS (nm)	Ra (nm)	R_{Sk}	R_{Ku}
40 × 40 µm	255	197	0.51	4.59

Figure 9 shows the analysis of the structure achieved after incorporating Au nanoparticles into the graphene—PANI-EB assembly. The presence of gold in the form of quasi-spherical particles with an average size of about 100 nm is clearly visible, yet the quantity of metallic particles is greater and somewhat grouped in small clusters.



(**a**) (**b**)

Figure 9. Optical analysis of graphene–PANI-EB+Au: (**a**) at 100× and (**b**) at 500×.

The grain size is generally 1.8 µm, in line with the dimension for graphene deposited with PANI-EB without Au addition, Figure 10. The grains are usually organized in larger groups. The R_{Sk} values are high, indicating the development of unique hollows after Au deposition, characterized by a specific arrangement featuring large hollows among the groups of grains. The R_{ku} values are over 7, demonstrating that the grain symmetry is completely altered by the inclusion of Au, as illustrated in Table 5, as integration of metal compels the initial grains to form gaps for Au particles to delve further and gather into small clusters, thereby sharpening the peaks.

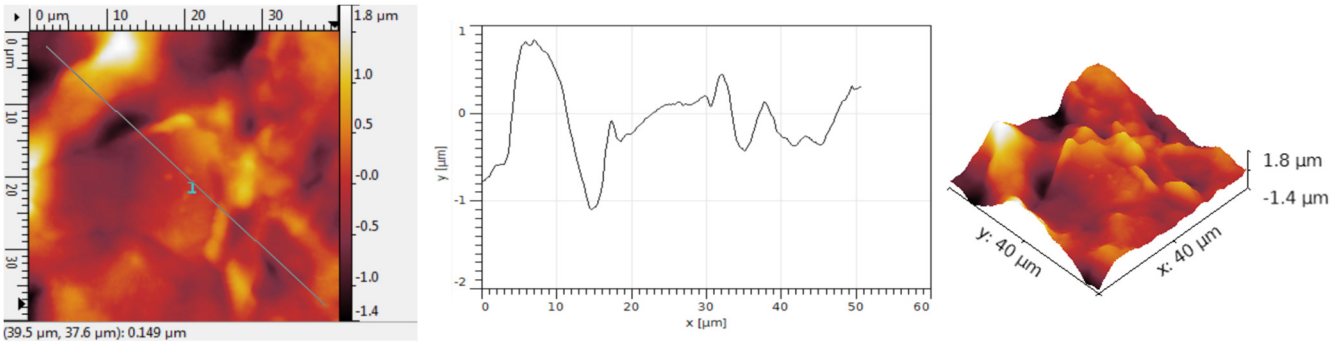
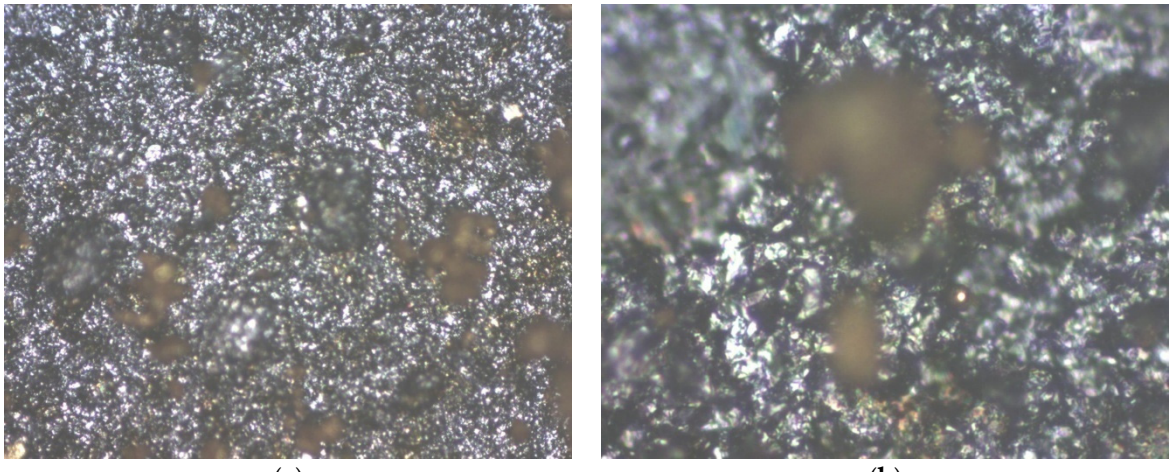


Figure 10. AFM Topographic image and profile lines for graphene–PANI-EB+Au.

Table 5. Average roughness parameters determined by AFM lines: graphene—PANI-EB+Au.

Scanned Area	RMS (nm)	Ra (nm)	R_{Sk}	R_{Ku}
40 × 40 µm	465	297	0.42	7.44

Figure 11 illustrates the analysis of the structure obtained after adding Au nanoparticles to the graphene–F8T2 composite. Gold is noticeably present. At first glance, when comparing Figures 7, 9 and 11, in this instance, the area covered with nanoparticles surpasses that of the graphene–P3HT assembly but is fewer compared to the graphene–PANI-EB assembly. The metallic particles are somewhat clustered in larger groups, but the respective clusters are quite dispersed among the graphene–F8T2 grains.



(**a**) (**b**)

Figure 11. Optical analysis of graphene–F8T2+Au: (**a**) at 100× and (**b**) at 500×.

The grain size typically reaches 3.8 µm, aligning with the dimensions for graphene deposited with F8T2 without the addition of Au, as shown in Figure 12. The grains are

typically arranged in smaller clusters. The low R_{Sk} values suggest the formation of some hollows; however, the architecture of these hollows is scattered, due to the fairly dispersed gold clusters, and overall, the grains settle closely together, resulting in minimal free space among them. The R_{ku} values exceed 4, indicating that the grain symmetry is somewhat modified by the presence of Au, as shown in Table 6, although this modification is less significant compared to the graphene–PANI-EB assembly case, since, despite clustering, the Au particle clusters are few and fairly dispersed.

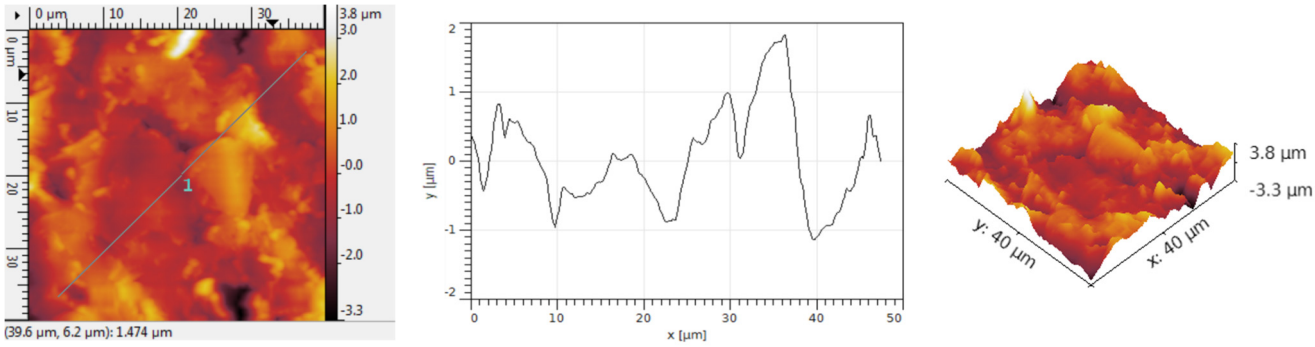


Figure 12. AFM Topographic image and profile lines for graphene–F8T2+Au.

Table 6. Average roughness parameters determined by AFM lines: graphene—F8T2+Au.

Scanned Area	RMS (nm)	Ra (nm)	R_{Sk}	R_{Ku}
40 × 40 µm	767	563	0.195	4.63

To evaluate the amount of gold in these hybrid structures, energy dispersive X-ray analyses were performed. The images have been very challenging to identify differences regarding the Au peak intensities, as there is a very low amount of gold relative to the graphene quantity, and minimal fluctuation in atomic percentage of gold as well, which renders the images irrelevant. Conversely, because of the weak EDS signal from small nanoparticles, the detection time for these particles increased, and other elements, such as Cu, Fe, and Co (likely connected to the sample holders etc.), appeared in the images, affecting the quality of the Au peak intensities. EDS analysis, a semi-quantitative method, has reasonably confirmed the incorporation of gold nanoparticles into hybrid structures. Table 7 depicts the weight and atomic percentage of gold atoms in the hybrid samples, but under the previously mentioned experimental conditions, the accuracy of this information is constrained.

Table 7. Weight and atomic percentage of gold atoms in the hybrid samples.

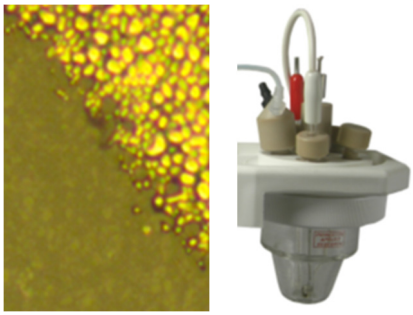
Hybrid Structure	Weight Percentage (%)	Atomic Percentage (%)
Graphene–P3HT+Au	3.79 ± 0.14	0.25 ± 0.05
Graphene–PANI-EB+Au	9.81 ± 0.16	0.65 ± 0.04
Graphene–F8T2+Au	6.02 ± 0.12	0.39 ± 0.08

In assessing the incorporation of gold nanoparticles into graphene-conducting polymer assemblies, we can infer that the interaction of gold with the polymer structures varies significantly, with P3HT exhibiting the weakest physical connection and lowest quantity of linked gold nanoparticles and PANI-EB showing the strongest. Conversely, the effect of incorporating gold nanoparticles varies, being more individual and dispersed for P3HT, and distinctly clustered and more agglomerated for the other two structures.

In every instance, a fairly symmetrical arrangement of grains was observed, with minimized space between them. Structures featuring symmetrical distribution and roughness dimensions at the micrometer scale are regarded as ideal for use as electrochemical sensors, although electrochemical evaluations in various reactants could determine their definitive usefulness.

3.2. Analysis of Electrochemical Functionality

The literature describes various metallization processes for graphene-supported composite materials, such as in [46], but many of them are unsuitable for a basic sensor application. In our instance, an ink-jet printer was utilized, and the metallization was performed using commercial ORGACON SI-J20X ink (Agfa-Gevaert N.V., Mortsel, Belgium) designed for printed electronics, by deposition in 2 layers. A uniform dispersion of the ink on the active area was observed, Figure 13a. An electrode structure was created from each of the earlier shown hybrid samples, featuring an active surface approximately 1–1.5 cm^2, linked on one side to the connecting conducting path.



(**a**) (**b**)

Figure 13. (**a**) Sample of working electrode; (**b**) K0264 Micro-Cell Kit configuration used as electrochemical cell assembly.

The electrochemical cell utilized for obtaining the cyclic voltammograms consisted of three electrodes: one of the previously mentioned electrodes served as the working electrode, the reference electrode was Silver/Silver chloride, and the counter electrode was a Pt spiral of 0.3 mm diameter. The K0264 Micro-Cell Kit configuration, used as electrochemical cell assembly, is presented in Figure 13b.

The solution employed for the preliminary testing the three working electrodes was a 0.5 M aqueous H_2SO_4 solution, a typical method associated with cyclic voltammetry for examining proton reduction [47–49], primarily if pertaining to electrodes that include metallic elements. Figure 14 displays the cyclic voltammograms of the graphene–P3HT electrode with Au nanoparticles, employing 3 scanning rates of: 200, 100, and 50 mV/s respectively.

A thorough examination of Figure 14 shows that the peaks of oxidation and reduction in the voltammograms are found at 439 and 325 mV, respectively, indicating an irreversible process related to the electrochemical doping of P3HT by HSO_4^- anions in the vicinity of Au nanoparticles, similar with the cases described in [50,51]. As the scanning speed slows down, a reduction in both the anodic and cathodic current densities of the voltammograms is noted.

Figure 15 presents the cyclic voltammograms of the graphene–PANI-EB electrode with Au nanoparticles, at the same scanning rates.

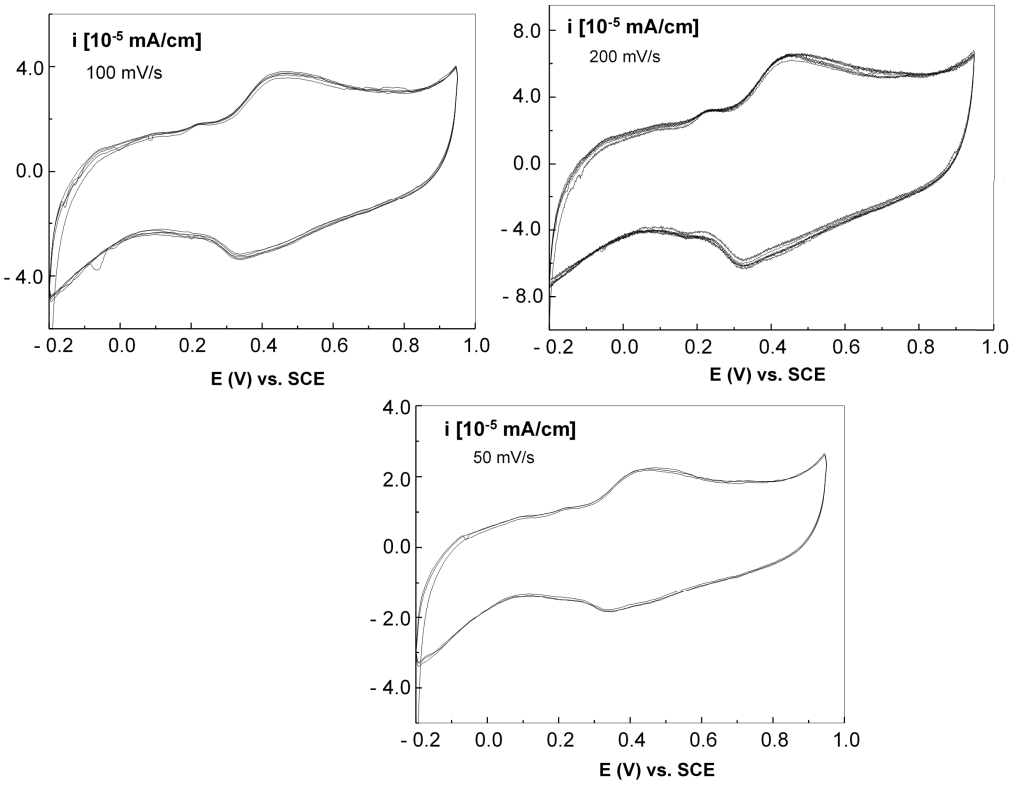


Figure 14. Cyclic voltammograms for graphene–P3HT+Au at scanning speeds of 200, 100, and 50 mV/s.

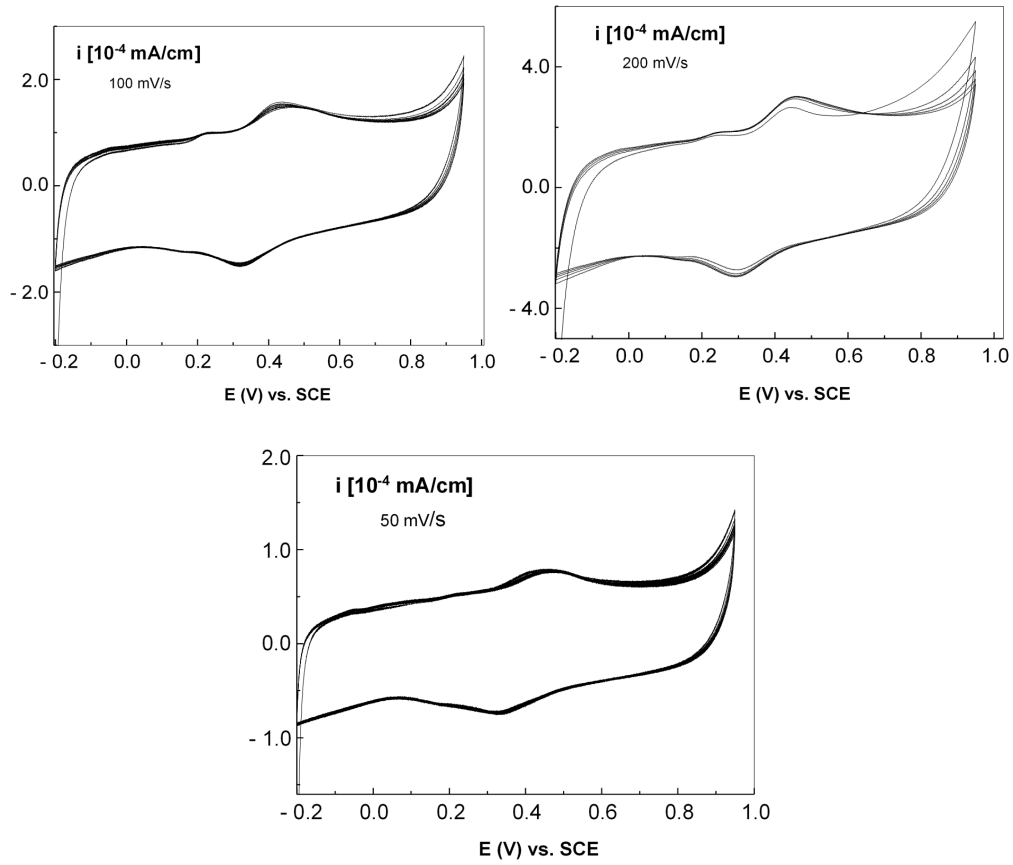


Figure 15. Cyclic voltammograms for graphene–PANI-EB+Au at scanning speeds of 200, 100, and 50 mV/s.

It was observed that regardless of the scanning speed, the cyclic voltammograms display an oxidation peak at 450 mV and a reduction peak at 291 mV. This difference in potential between the maximum oxidation and reduction indicates an irreversible process resulting from the doping of PANI-EB, which leads to the creation of emeraldine polyaniline salt (PANI-ES). Furthermore, as the scanning speed decreases, there is a nearly linear drop in the anodic and cathodic current densities, suggesting that the electrochemical process is controlled by diffusion.

Finally, Figure 16 presents the cyclic voltammograms of the graphene– F8T2 electrode with Au nanoparticles, at the same scanning rates.

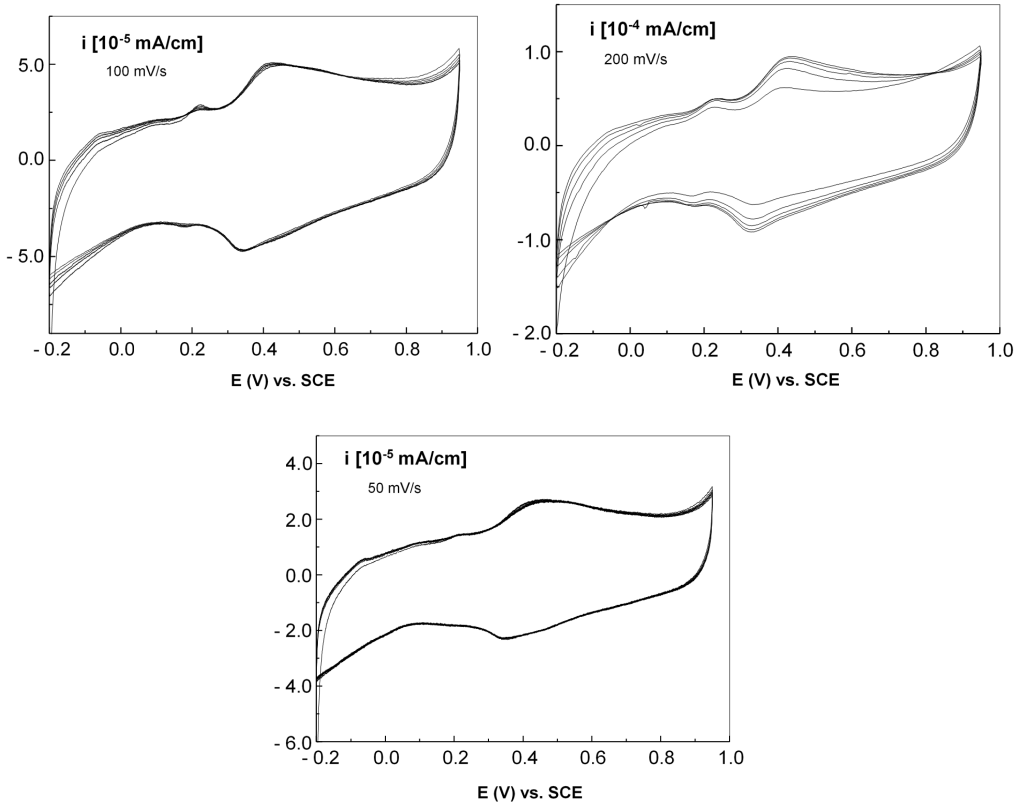


Figure 16. Cyclic voltammograms for graphene–F8T2+Au at scanning speeds of 200, 100, and 50 mV/s.

Upon examining the voltammograms collected at a sweep rate of 200 mV/s, it is evident that the maximum anodic and cathodic current densities increase with a growing number of cyclic voltammograms. By the conclusion of the 5 cycles, the process generally starts to stabilize, with the oxidation and reduction potentials of 428 and 325 mV, respectively. This effect is reduced at slower scanning speeds. More than this, a slower sweep speed leads to a decreased density of the anodic and cathodic currents, with a slight shift in the positions of the oxidation and reduction peaks; at a sweep speed of 50 mV/s, the potentials of the anodic and cathodic maxima are 448 mV and 337 mV, respectively. The voltage variation linked to the anodic and cathodic peaks suggests an irreversible process tied to the doping of the F8T2 macromolecular compound with gold nanoparticles, especially concerning their clustering in large quantities.

In all cases, especially at higher scanning speeds, preliminary minor oxidation and reduction processes, at potentials of about 200 and 180 mV, respectively, were noticed. They can be explained by the surface oxidation of gold nanoparticles, especially if pertaining to electrodes that include a carbon-based support, as described e.g., in [52]. A piece of evidence supporting this hypothesis is that for the graphene–F8T2 electrode, the effect

is somewhat intensified when taking into account the clustering of Au nanoparticles in greater amounts. The variations of the electrochemical features demonstrated by the three electrodes when exposed to the 0.5 M H_2SO_4 solution distinctly show that the oxidation and reduction reactions at the electrode/electrolyte interface possess an irreversible nature due to the doping of the conjugated polymers, enhanced by the presence of gold nanoparticles.

The notable differences in roughness (grain size) and the arrangement of Au nanoparticles distribution within polymer grains lead to differing behaviors of those structures, and thus, any possible discrepancies in the sensitivity of the created sensing structures can be further clarified by this spatial configuration. At first glance, the oxidation and reduction potentials of the structures appear quite similar, particularly in the presence of sulfuric acid solution. However, a significant distinction can be observed in the values of the anodic and cathodic current densities, which seem to be greatly influenced by the amount and the way the gold nanoparticles are attached to the polymeric grains. In examining the slight oxidation and reduction reactions of Au nanoparticles for graphene–P3HT assembly, the effect appears comparable to that observed for graphene-F8T2 assembly, despite a noticeable difference in the atomic percentage of Au nanoparticles attached to each polymer surface, Table 7. Conversely, the oxidation and reduction processes of Au nanoparticles are hardly significant for the graphene–PANI-EB assembly, despite the amount of Au nanoparticles attached to the respective polymer surface being similar to that of the graphene-F8T2 assembly. For graphene–P3HT and graphene-F8T2 assemblies, the incorporation of Au nanoparticles appears to provide a distinct effect that does not necessarily improve the polymer's electrochemical activity. In contrast, for the graphene–PANI-EB assembly, the impact is more synergistic, the oxidation and reduction processes of Au nanoparticles being negligible. These findings are supported by the analysis of Au nanoparticle dispersion linked to Figures 7, 9 and 11, where a more uniform and consistent distribution of Au nanoparticles among the polymer grains is observed solely in the case of the graphene–PANI-EB assembly.

In Figure 17, the current densities of structures at different scanning speeds is presented for the three graphene-polymer assemblies. The tests were repeated five times, and the results presented achieved a confidence level exceeding 90%. As shown, the most responsive structure is validated to be graphene–PANI-EB integrating Au nanoparticles. The explanation is founded on an adequately large grain size of 1.8 μm of the structure, with a significant quantity of Au nanoparticles, arranged as small clusters uniformly dispersed among the polymer grains, which become sharper due to arrangement of Au nanoparticles.

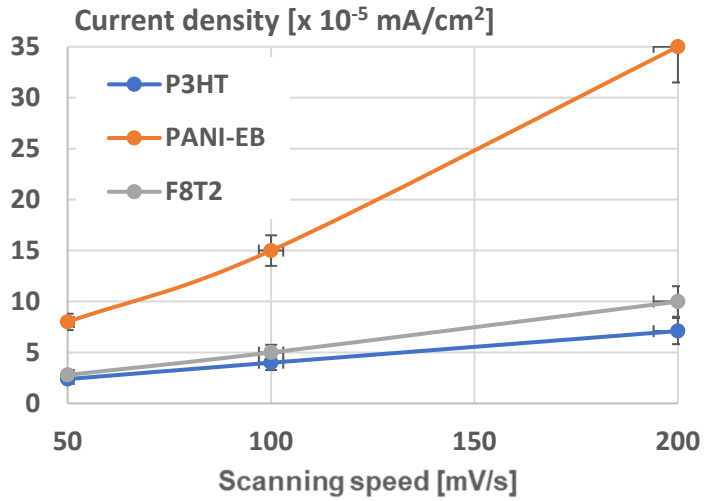


Figure 17. Current densities of structures at different scanning speeds.

In contrast to other research on graphene-polyaniline composites that may serve as electrochemical sensors [53–57], which primarily focus on graphene clusters embedded within PANI chains and utilize Van der Waals interactions on larger surfaces, the electrode technology introduced in this paper is groundbreaking and highlights a novel approach in altering at the nanoscale the architecture of sensing structures traditionally composed solely of graphene and conducting polymers. Additionally, incorporating gold nanoparticles enhances sensitivity regarding redox potential, both of which are critical attributes for an electrochemical sensor that targets specific biomolecular components for testing. Future research will focus on specifying hybrid structures of graphene–PANI-EB integrating Au nanoparticles for cancer diagnosis, aiming to exceed the results presented in [58,59], where the properties of PANI and graphene are examined independently, or the results presented in [60–63], where gold nanoparticles and graphene are examined independently.

4. Conclusions

This paper describes the process of fabricating electrodes utilizing hybrid nanostructures made from graphene and conductive polymers, as well as integrating gold nanoparticles.

The technique employed to create hybrid nanostructures from graphene and conducting polymers was drop-casting, using solutions of P3HT, PANI-EB, and F8T2. Furthermore, the graphene-conducting polymer structures were submerged in a $HAuCl_4$/2-propanol solution employing a novel dip-coating method, followed by a controlled heating from room temperature to just above one hundred degrees Celsius. The technique offers the benefit of generating and quasi-uniformly distributing gold nanoparticles with an average size of 100 nm across larger graphene-polymer structure surfaces. The incorporation of gold nanoparticles into polymer structures varies significantly, as P3HT shows the least affinity while PANI-EB exhibits the greatest.

An ink-jet printer was utilized to fabricate electrodes for electrochemical experiments from the relevant hybrid structures, with metallization carried out using commercially available silver ink intended for printed electronics. The electrochemical experiments used a 0.5 M aqueous $H2SO_4$ solution at three different scanning rates. The significant difference in roughness (grain size) leads to diverse behaviors of these structures, and thus, any possible variation in sensitivity can be better comprehended through this spatial configuration. At a glance, the oxidation and reduction potentials of the structures appear quite similar. However, a significant distinction is observable in the anodic and cathodic current density values, which seem to be greatly influenced by the active surface and structure of gold nanoparticles attached to the polymeric grains. The most responsive structure seems to be graphene–PANI-EB with Au nanoparticles, featuring a grain size of 1.8 μm and a significant quantity of Au nanostructures, arranged in small clusters that are evenly spread across the polymer grains.

Upcoming studies will target the specification of this electrode type for cancer detection.

Author Contributions: Conceptualization, A.F.T., R.C.C. and O.D.S.; methodology, R.C.C., O.D.S. and T.G.S.; validation, R.C.C., T.G.S. and A.F.T.; formal analysis, A.F.T., O.P. and R.C.C.; investigation, R.C.C., O.D.S., T.G.S., O.P. and A.F.T.; data curation, R.C.C., O.D.S., T.G.S., O.P. and A.F.T.; writing—original draft preparation, A.F.T. and R.C.C.; writing—review and editing, R.C.C.; visualization, R.C.C., O.D.S. and A.F.T.; supervision, A.F.T. and R.C.C. All authors have read and agreed to the published version of the manuscript.

Funding: This research received no external funding.

Institutional Review Board Statement: Not applicable.

Informed Consent Statement: Not applicable.

Data Availability Statement: Data are contained within the article.

Conflicts of Interest: The authors declare no conflicts of interest.

References

1. Zamiri, G.; Haseeb, A.S.M.A. Recent Trends and Developments in Graphene/Conducting Polymer Nanocomposites Chemiresistive Sensors. *Materials* **2020**, *13*, 3311. [CrossRef] [PubMed]
2. Cai, X.; Sun, K.; Qiu, Y.; Jiao, X. Recent Advances in Graphene and Conductive Polymer Composites for Supercapacitor Electrodes: A Review. *Crystals* **2021**, *11*, 947. [CrossRef]
3. Bai, H.; Sheng, K.; Zhang, P.; Li, C.; Shi, G. Graphene oxide/conducting polymer composite hydrogels. *J. Mater. Chem.* **2011**, *21*, 18653–18658. [CrossRef]
4. Conducting Polymer/Graphene-Based Material Composites, and Methods for Preparing the Composites. Available online: https://patents.google.com/patent/US20140087192A1/en (accessed on 12 March 2024).
5. Chauhan, A.K.; Gupta, S.K.; Taguchi, D.; Manaka, T.; Jha, P.; Veerender, P.; Sridevi, C.; Koiry, S.P.; Gadkari, S.C.; Iwamoto, M. Enhancement of the carrier mobility of conducting polymers by formation of their graphene composites. *RSC Adv.* **2017**, *7*, 11913–11920. [CrossRef]
6. Kausar, A. Conjugated Polymer/Graphene Oxide Nanocomposites—State-of-the-Art. *J. Compos. Sci.* **2021**, *5*, 292. [CrossRef]
7. Sharma, S.; Sudhakara, P.; Omran, A.A.B.; Singh, J.; Ilyas, R.A. Recent Trends and Developments in Conducting Polymer Nanocomposites for Multifunctional Applications. *Polymers* **2021**, *13*, 2898. [CrossRef]
8. Dunlop, M.J.; Bissessur, R. Nanocomposites based on graphene analogous materials and conducting polymers: A review. *J. Mater. Sci.* **2020**, *55*, 6721–6753. [CrossRef]
9. Adedoja, O.S.; Sadiku, E.R.; Hamam, Y. Prospects of Hybrid Conjugated Polymers Loaded Graphene in Electrochemical Energy Storage Applications. *J. Inorg. Organomet. Polym. Mater.* **2023**, *33*, 3915–3934. [CrossRef]
10. Shalini, A.; Kothai, S.; Jaisankar, V. Graphene Deposited Conducting Polymers: Synthesis and Sensing Applications. *Int. J. Curr. Res. Aca. Rev.* **2021**, *9*, 94–103. [CrossRef]
11. Zhu, Z.; Lin, W.-D.; Lin, Z.-Y.; Chuang, M.-H.; Wu, R.-J.; Chavali, M. Conductive Polymer (Graphene/PPy)–$BiPO_4$ Composite Applications in Humidity Sensors. *Polymers* **2021**, *13*, 2013. [CrossRef]
12. Das, P.; Chakraborty, K.; Pan, A.; Ghosh, S.; Pal, T. Conductivity relaxation and photocurrent generation in reduced graphene oxide-poly(9,9′-dioctyl-fluorene-co-bithiophene) composite with application in temperature sensing. *J. Appl. Phys.* **2019**, *125*, 085104. [CrossRef]
13. Pinelli, F.; Nespoli, T.; Fiorati, A.; Farè, S.; Magagnin, L.; Rossi, F. Graphene nanoplatelets can improve the performances of graphene oxide—Polyaniline composite gas sensing aerogels. *Carbon Trends* **2021**, *5*, 100123. [CrossRef]
14. Lee, S.J.; Yoon, S.J.; Jeon, I.-Y. Graphene/Polymer Nanocomposites: Preparation, Mechanical Properties, and Application. *Polymers* **2022**, *14*, 4733. [CrossRef]
15. Cheng, S.; Wang, Y.; Zhang, R.; Wang, H.; Sun, C.; Wang, T. Recent Progress in Gas Sensors Based on P3HT Polymer Field-Effect Transistors. *Sensors* **2023**, *23*, 8309. [CrossRef] [PubMed]
16. Cheon, H.J.; Shin, S.Y.; Van Tran, V.; Park, B.; Yoon, H.; Chang, M. Preparation of conjugated polymer/reduced graphene oxide nano-composites for high-performance volatile organic compound sensors. *Chem. Eng. J.* **2021**, *425*, 131424. [CrossRef]
17. Khanh, T.S.T.; Trung, T.Q.; Giang, L.T.T.; Nguyen, T.Q.; Lam, N.D.; Dinh, N.N. Ammonia Gas Sensing Characteristic of P3HT-rGO-MWCNT Composite Films. *Appl. Sci.* **2021**, *11*, 6675. [CrossRef]
18. Verma, A.; Gupta, R.; Verma, A.S.; Kumar, T. A review of composite conducting polymer-based sensors for detection of industrial waste gases. *Sens. Actuators Rep.* **2023**, *5*, 100143. [CrossRef]
19. Lei, W.; Si, W.; Xu, Y.; Gu, Z.; Hao, Q. Conducting polymer composites with graphene for use in chemical sensors and sensors. *Microchim. Acta* **2014**, *181*, 707–722. [CrossRef]
20. Kim, Y.; An, T.K.; Kim, J.; Hwang, J.; Park, S.; Nam, S.; Cha, H.; Park, W.J.; Baik, J.M.; Park, C.E. A composite of a graphene oxide derivative as a novel sensing layer in an organic field-effect transistor. *J. Mater. Chem. C* **2014**, *2*, 4539–4544. [CrossRef]
21. Rahman, A.; Pal, R.K.; Islam, N.; Freeman, R.; Berthiaume, F.; Mazzeo, A.; Ashraf, A. A Facile Graphene Conductive Polymer Paper Based Sensor for Dopamine, TNF-α, and IL-6 Detection. *Sensors* **2023**, *23*, 8115. [CrossRef]
22. Kumar, A.; Gupta, G.H.; Singh, G.; More, N.; Keerthana, M.; Sharma, A.; Jawade, D.; Balu, A.; Kapusetti, G. Ultrahigh sensitive graphene oxide/conducting polymer composite based sensor for cholesterol and bilirubin detection. *Biosens. Bioelectron. X* **2023**, *13*, 100290. [CrossRef]
23. Al-Graiti, W.; Foroughi, J.; Liu, Y.; Chen, J. Hybrid Graphene/Conducting Polymer Strip Sensors for Sensitive and Selective Electrochemical Detection of Serotonin. *ACS Omega* **2019**, *4*, 22169–22177. [CrossRef] [PubMed]
24. Văduva, M.; Baibarac, M.; Cramariuc, O. Functionalization of Graphene Derivatives with Conducting Polymers and Their Applications in Uric Acid Detection. *Molecules* **2023**, *28*, 135. [CrossRef]

25. Song, J.; Kim, Y.; Kang, K.; Lee, S.; Shin, M.; Son, D. Stretchable and Self-Healable Graphene–Polymer Conductive Composite for Wearable EMG Sensor. *Polymers* **2022**, *14*, 3766. [CrossRef] [PubMed]
26. DiFrancesco, M.L.; Colombo, E.; Papaleo, E.D.; Maya-Vetencourt, J.F.; Manfredi, G.; Lanzani, G.; Benfenati, F. A hybrid P3HT-Graphene interface for efficient photostimulation of neurons. *Carbon* **2020**, *162*, 308–317. [CrossRef]
27. Yazid, S.N.A.M.; Adnan, A.A.C.; Isa, I.M.; Saidin, M.I.; Ahmad, M.S.; Fun, C.S. Conducting polymer functionalized graphene-based electrochemical sensors for sensing pollutants in water. *J. Electrochem. Sci. Eng.* **2023**, *13*, 251–274. [CrossRef]
28. Diédhiou, I.; Fall, B.; Gaye, C.; Sall, M.L.; Diaw, A.K.D.; Gningue-Sall, D.; Fall, M.; Raouafi, N. Preparations and applications of organic conducting polymers/graphene composites in heavy metal ion sensing: A review. *Int. J. Mater. Res.* **2023**, *114*, 79–99. [CrossRef]
29. Lin, C.-H.; Lin, J.-H.; Chen, C.-F.; Ito, Y.; Luo, S.-C. Conducting polymer-based sensors for food and drug analysis. *J. Food Drug Anal.* **2021**, *29*, 544–558. [CrossRef]
30. Mulyono, T.; Siswoyo, A.; Lestari, P.B.; Zulfikar; Mufliha, Y.M. Development of A Resistive Sensor Array Based on Graphene and Conducting Polymer Composites for Coffee Aroma Classification. In Proceedings of the International Conference on Sustainable Chemistry (ICSChem 2023), Malang, Indonesia, 22–23 August 2023; Volume 481, p. 06012. [CrossRef]
31. Avelino, K.Y.; Oliveira, L.S.; Lucena-Silva, N.; Andrade, C.A.; Oliveira, M.D. Flexible sensor based on conducting polymer and gold nanoparticles for electrochemical screening of HPV families in cervical specimens. *Talanta* **2021**, *226*, 122118. [CrossRef] [PubMed]
32. Avelino, K.; Oliveira, L.; Lucena-Silva, N.; de Melo, C.; Andrade, C.; Oliveira, M. Metal-polymer hybrid nanomaterial for impedimetric detection of human papillomavirus in cervical specimens. *J. Pharm. Biomed. Anal.* **2020**, *185*, 113249. [CrossRef] [PubMed]
33. Rahman, A.; Son, J.I.; Won, M.-S.; Shim, Y.-B. Gold Nanoparticles Doped Conducting Polymer Nanorod Electrodes: Ferrocene Catalyzed Aptamer-Based Thrombin Immunosensor. *Anal. Chem.* **2009**, *81*, 6604–6611. [CrossRef] [PubMed]
34. Yan, Y.; Yang, G.; Xu, J.-L.; Zhang, M.; Kuo, C.-C.; Wang, S.-D. Conducting polymer-inorganic nanocomposite-based gas sensors: A review. *Sci. Technol. Adv. Mater.* **2020**, *21*, 768–786. [CrossRef]
35. Fabregat, G.; Armelin, E.; Alemán, C. Selective Detection of Dopamine Combining Multilayers of Conducting Polymers with Gold Nanoparticles. *J. Phys. Chem. B* **2014**, *118*, 4669–4682. [CrossRef] [PubMed]
36. Kumalasari, M.; Alfanaar, R.; Andreani, A. Gold nanoparticles (AuNPs): A versatile material for sensor application. *Talanta Open* **2024**, *9*, 100327. [CrossRef]
37. Petrucci, R.; Bortolami, M.; Di Matteo, P.; Curulli, A. Gold Nanomaterials-Based Electrochemical Sensors and Sensors for Phenolic Antioxidants Detection: Recent Advances. *Nanomaterials* **2022**, *12*, 959. [CrossRef]
38. Hou, J.; Li, B.; Jang, W.; Yun, J.; Eyimegwu, F.M.; Kim, J.-H. Integration of Gold Nanoparticles into Crosslinker-Free Polymer Particles and Their Colloidal Catalytic Property. *Nanomaterials* **2023**, *13*, 416. [CrossRef]
39. Hou, J.; Yun, J.; Jang, W.; Li, B.; Adehinmoye, A.A.; Kim, J.-H.; Byun, H. Rapid incorporation of gold nanoparticles onto graphene oxide-polymer nanofiber membranes for photothermally-accelerated water purification. *J. Polym. Eng.* **2022**, *43*, 156–166. [CrossRef]
40. Chekkaramkodi, D.; El Turk, S.; Ali, M.; Butt, H. In-situ synthesis and integration of gold nanoparticles into 3D printed optical fiber probes. *Sci. Rep.* **2024**, *14*, 29736. [CrossRef]
41. Trandabat, A.F.; Ciobanu, R.C.; Schreiner, O.D.; Schreiner, T.G.; Aradoaei, S. Chemiresistors Based on Hybrid Nanostructures Obtained from Graphene and Conducting Polymers with Potential Use in Breath Methane Detection Associated with Irritable Bowel Syndrome. *Int. J. Mol. Sci.* **2024**, *25*, 5552. [CrossRef]
42. Umeda, H.; Mezaki, Y.; Oshio, A.; Kaneko, Y.; Okamoto, R.; Kusumoto, S.; Kunimura, S. Gold Nanoparticles Produced by Low-temperature Heating of the Dry Residue of a Droplet of an HCl Acidic Solution of $HAuCl_4 \cdot 4H_2O$ in a Low Vacuum. *Anal. Sci.* **2021**, *37*, 1427–1432. [CrossRef]
43. Ii, K.; Kurita, Y.; Kida, N.; Kunimura, S. Preparation of gold nanoparticles using low-temperature heating of the dry residue of a droplet of an HAuCl4 solution in air. *Anal. Sci.* **2024**, *40*, 213–217. [CrossRef]
44. Surface Roughness Parameters. Available online: https://www.keyence.eu/ss/products/microscope/roughness/line/tab03_b.jsp (accessed on 20 November 2024).
45. *ISO 21920-2:2021 (previously ISO 4287:1997)*; Geometrical Product Specifications (GPS)—Surface Texture: Profile—Part 2: Terms, Definitions and Surface Texture Parameters. International Organization for Standardization: Geneva, Switzerland, 2021. Available online: https://www.iso.org/standard/72226.html (accessed on 20 November 2024).
46. Rafailović, L.D.; Jovanović, A.Z.; Gutić, S.J.; Wehr, J.; Rentenberger, C.; Trišović, T.L.; Pašti, I.A. New Insights into the Metallization of Graphene-Supported Composite Materials–from 3D Cu-Grown Structures to Free-Standing Electrodeposited Porous Ni Foils. *ACS Omega* **2022**, *7*, 4352–4362. [CrossRef]
47. Zeng, Q.; Xia, K.; Zhang, Y.; Wu, T. Well Controlled 3D Iridium Oxide/Platinum Nanocomposites with Greatly Enhanced Electrochemical Performances. *Adv. Mater. Interfaces* **2019**, *6*, 1900356. [CrossRef]

48. Tamilselvi, B.; Bhuvaneshwari, D.S.; Karuppasamy, P.; Padmavathy, S.; Nikhil, S.; Siddegowda, S.B.; Murthy, H.C.A. Investigation of Corrosion Inhibition of Mild Steel in 0.5 M H2SO4 with Lachancea fermentati Inhibitor Extracted from Rotten Grapefruits (*Vitis vinifera*): Adsorption, Thermodynamic, Electrochemical, and Quantum Chemical Studies. *ACS Phys. Chem. Au* **2024**, *4*, 67–84. [CrossRef] [PubMed]
49. Zhong, W.; Xiao, B.; Lin, Z.; Wang, Z.; Huang, L.; Shen, S.; Zhang, Q.; Gu, L. $RhSe_2$: A Superior 3D Electrocatalyst with Multiple Active Facets for Hydrogen Evolution Reaction in Both Acid and Alkaline Solutions. *Adv. Mater.* **2021**, *33*, 2007894. [CrossRef] [PubMed]
50. Choi, W.; Bard, A. Doping of the Semiconducting Polymer Poly(3-hexylthiophene) (P3HT) in Organic Photoelectrochemical Cells. *J. Phys. Chem. C* **2020**, *124*, 3439–3447. [CrossRef]
51. Zhao, D.; Li, L.; Niu, W.; Chen, S. Highly conductive polythiophene films doped with chloroauric acid for dual-mode sensing of volatile organic amines and thiols. *Sens. Actuators B Chem.* **2017**, *243*, 380–387. [CrossRef]
52. Wang, Y.; Laborda, E.; Crossley, A.; Compton, R.G. Surface oxidation of gold nanoparticles supported on a glassy carbon electrode in sulphuric acid medium: Contrasts with the behaviour of 'macro' gold. *Phys. Chem. Chem. Phys.* **2013**, *15*, 3133–3136. [CrossRef]
53. Farooqi, B.A.; Yar, M.; Ashraf, A.; Farooq, U.; Ayub, K. Graphene-polyaniline composite as superior electrochemical sensor for detection of cyano explosives. *Eur. Polym. J.* **2020**, *138*, 109981. [CrossRef]
54. Wei, L.; Fan, L.; Yang, H.; Wu, Y. Graphene/Polyaniline Nanocomposite as an Electrochemical Sensor for Ultrasensitive Detection of Pb(II). *Int. J. Electrochem. Sci.* **2019**, *14*, 10720–10728. [CrossRef]
55. Hadano, F.S.; Gavim, A.E.X.; Stefanelo, J.C.; Gusso, S.L.; Macedo, A.G.; Rodrigues, P.C.; Yusoff, A.R.b.M.; Schneider, F.K.; de Deus, J.F.; da Silva, W.J. NH_3 Sensor Based on rGO-PANI Composite with Improved Sensitivity. *Sensors* **2021**, *21*, 4947. [CrossRef] [PubMed]
56. Xie, A.; Du, J.; Zhang, J.; Xiong, Z.; Shao, F.; Luo, S. A High-Performance Nonenzymatic Urea Sensor Based on Graphene-NiO-Polyaniline. *J. Electrochem. Soc.* **2019**, *166*, B456. [CrossRef]
57. Santos-Ceballos, J.C.; Salehnia, F.; Güell, F.; Romero, A.; Vilanova, X.; Llobet, E. Room-Temperature Ammonia Sensing Using Polyaniline-Coated Laser-Induced Graphene. *Sensors* **2024**, *24*, 7832. [CrossRef] [PubMed]
58. Hosseine, M.; Bakhshi, A.; Naghib, S.M.; Rabiee, N. Recent advancements in polyaniline-based sensors for diagnosis of cancers: A comprehensive review. *TrAC Trends Anal. Chem.* **2024**, *181*, 118040. [CrossRef]
59. Al-Salman, H.; Hsu, C.-Y.; Jawad, Z.N.; Mahmoud, Z.H.; Mohammed, F.; Saud, A.; Al-Mashhadani, Z.I.; Abu Hadal, L.S.; Kianfar, E. Graphene oxide-based sensors for detection of lung cancer: A review. *Results Chem.* **2024**, *7*, 101300. [CrossRef]
60. Pothipor, C.; Jakmunee, J.; Bamrungsap, S.; Ounnunkad, K. An electrochemical sensor for simultaneous detection of breast cancer clinically related microRNAs based on a gold nanoparticles/graphene quantum dots/graphene oxide film. *Analyst* **2021**, *146*, 4000–4009. [PubMed]
61. Li, Y.; Wang, X.; Wang, X.; Qin, Z.; Li, C.; Yang, J.; Cao, M. Electrochemical sensor based on composite of gold nanoparticle/reduced-graphene oxide/graphitic carbon nitride and a caprolactone polymer for highly sensitive detection of CEA. *Bioelectrochemistry* **2025**, *163*, 108897. [CrossRef]
62. Li, C.-H.; Chan, M.-H.; Chang, Y.-C.; Hsiao, M. Gold Nanoparticles as a Sensor for Cancer Biomarker Determination. *Molecules* **2023**, *28*, 364. [CrossRef]
63. Gao, C.; Jiang, Z. Gold Nanoparticles (Aunps)-Based Sensors for Cancer Detection. *Trans. Mater. Biotechnol. Life Sci.* **2024**, *4*, 31–35. [CrossRef]

Disclaimer/Publisher's Note: The statements, opinions and data contained in all publications are solely those of the individual author(s) and contributor(s) and not of MDPI and/or the editor(s). MDPI and/or the editor(s) disclaim responsibility for any injury to people or property resulting from any ideas, methods, instructions or products referred to in the content.